IOPscience iopscience.iop.org

Home Search Collections Journals About Contact us My IOPscience

Influence of the short-range structural properties on the elastic constants of Si/Ge superlattices

This article has been downloaded from IOPscience. Please scroll down to see the full text article.

2000 J. Phys.: Condens. Matter 12 2931

(http://iopscience.iop.org/0953-8984/12/13/305)

View the table of contents for this issue, or go to the journal homepage for more

Download details:
IP Address: 171.66.16.221
The article was downloaded on 16/05/2010 at 04:43

Please note that terms and conditions apply.

J. Phys.: Condens. Matter **12** (2000) 2931–2943. Printed in the UK PII: S0953-8984(00)07439-7

Influence of the short-range structural properties on the elastic constants of Si/Ge superlattices

C Prieto†, A de Bernabé†, R Castañer‡, A Muñoz-Martín†, R J Jiménez-Rioboó†, M García-Hernández† and A de Andrés†

† Instituto de Ciencia de Materiales de Madrid, Consejo Superior de Investigaciones Científicas, Cantoblanco, E-28049 Madrid, Spain

‡ Departamento de Ciencia y Tecnología de Materiales, Universidad Miguel Hernández, Avenida del Ferrocarril s/n E-03202, Elche, Spain

Received 2 September 1999, in final form 18 January 2000

Abstract. The elastic constant tensor of Si_m/Ge_n superlattices with different modulation wavelengths has been determined by Brillouin light scattering spectroscopy. The C_{11} elastic constant obtained for Si_n/Ge_n (where bilayers are built up by an equal number of Si and Ge monolayers) and Si_n/Ge_{4n} superlattices are 13% above the predictions of the continuum elasticity theory, using the C_{ij} values of bulk Si and Ge. On the other hand, the elastic constant tensor of Si_{4n}/Ge_n and Si_{3n}/Ge_n superlattices matches perfectly the predictions. A structural analysis by extended x-ray absorption fine structure spectroscopy of the interfaces has been carried out and the unexpected different elastic behaviour can be explained by the observed strains at the superlattice interfaces.

1. Introduction

Si/Ge superlattice (SL) structures have been used successfully in some new devices such as heterojunction bipolar transistors. In particular, Si/Ge structures with very short period are especially interesting, since they can exhibit new optical properties different from bulk alloy materials. These new optical properties can be explained by zone folding effect of acoustic phonons [1].

Additionally, Si/Ge strained-layer SLs are of much interest from the point of view of band engineering through lattice strain and band alignment. For short period superlattices, the microstructure of interfaces can have much influence on the optical properties [2]. From this point of view, the short order structural characterization may give data on the interface quality as a function of the modulation wavelength.

Acoustic phonons are related to the elastic properties of solids. During the last years there has been controversy on the presence and origin of elastic constant anomalies in superlattices [3]. For many superlattice systems, there has been reported an anomalous behaviour of the surface acoustic waves (SAWs) in such a way that there is a dependence of the surface sound velocity (which is related to the C_{44} elastic constant) on the bilayer thickness. This experimental fact is in disagreement with the calculated behaviour by the theory of elasticity: the calculated elastic constant for a superlattice should be independent of the modulation wavelength. These predicted values are confirmed only in the case of long wavelength modulation samples. Many metallic SLs have been studied but, in contrast, no special attention has been paid to semiconductor superlattices. An interesting example is the Cu/Ni system, for

0953-8984/00/132931+13$30.00 © 2000 IOP Publishing Ltd

which was predicted a biaxial modulus (Y_B) value for samples with a modulation wavelength about 20 Å, even higher than that corresponding to diamond [4]. In contrast to what it is observed in sputtered samples that do not show any elastic difference, a dependence of the elastic constants on the modulation wavelength and a very large hardness for single-crystal (111) Cu/Ni superlattices was reported for samples prepared by the molecular beam epitaxy technique [5].

For some superlattice systems, the C_{44} elastic constant anomaly has been correlated to the so-called average lattice parameter, which takes into account the distances between planes of the superlattice [6]. On the other hand, the microstructural columnar growth has been used to formulate a geometrical model to reproduce the values of the whole elastic tensor in In–Ga–As ternary films [7]. Therefore, it can be concluded that elastic properties are fully related to the structural features of these materials.

Si/Ge superlattices are a very good system in order to study such a kind of anomalous behaviour because, in principle, samples are high quality single crystals and because the lattice mismatch between Si and Ge does not force the system to change the structural phase. The induced strain may have some influence on the elastic constants of these superlattices. In this sense, they are similar to the Cu/Ni system where both metals have an fcc structure with slightly different lattice parameters.

The elastic constants of thin films are usually determined by means of Brillouin light scattering (BLS) spectroscopy. It has two important advantages compared to other elastic probing techniques. First, the low penetration of light inside opaque materials permits us to discard any appreciable contribution from the substrate. This fact means that it is not necessary to remove the films from the substrate to evaluate their elastic properties. Second, there is no need of mechanical contacts to perform experiments, which is of interest in order to not damage the sample.

We have studied Si/Ge superlattices by BLS spectroscopy in order to determine their elastic constant tensor and the existence or not of some anomaly in their elastic constants (or dependence on the modulation wavelength). In addition, the same samples have been studied by means of x-ray absorption spectroscopy (XAS). XAS has been performed at the Ge K edge in order to determine the nearest neighbour Ge–Ge and Ge–Si distances and also to study the Ge/Si interface by the influence of the Ge–Si contribution to the extended x-ray absorption fine structure (EXAFS) signal. The aim of this paper is to relate the Ge layer and the Ge–Si interface short range structural properties with the elastic properties of the Si/Ge superlattices.

2. Experiment

Samples were prepared by molecular beam epitaxy in Professor Wang's group at the University of California Los Angeles. A complete description of the growth procedure has been given elsewhere [8]. The samples' structure is as follows: on an Si(001) substrate a 1000 Å Si layer was deposited over which a 2000 Å Si_xGe_{1-x} buffer was grown in order to have a good lattice match and a subsequent high degree of crystallinity. On top, the Si/Ge SL was grown having a total thickness of 3000 Å.

The studied samples, having Si/Ge ratios 1/1, 4/1, 3/1 and 1/4, are denoted as $(Si_n/Ge_m)_p$, where n, m and p are the number of Si monolayers, Ge monolayers and superlattice bilayers respectively. Samples are: $(Si_{20}/Ge_{20})_{55}$, $(Si_{15}/Ge_{15})_{73}$, $(Si_{10}/Ge_{10})_{110}$, $(Si_5/Ge_5)_{217}$, $(Si_{16}/Ge_4)_{120}$, $(Si_{32}/Ge_8)_{60}$, $(Si_{12}/Ge_4)_{80}$, and $(Si_4/Ge_{16})_{120}$. Samples have been selected to have the same total thickness in order to avoid any possible difference due to the self-absorption effect in XAS spectroscopy. Additionally, the same total thickness makes an easy comparison for the elastic behaviour.

BLS spectroscopy experimental set-up can be described as follows: The monochromatic source of light used was a 2060 Beamlok Spectra Physics Ar^+ laser. It is provided with an intracavity temperature stabilized single mode and single-frequency z-lok etalon. The selected wavelength was 514.5 nm with an incident power of about 100 mW. The spectrometer used was a JRS tandem Sandercock-type 3 + 3 pass [9]. The incident polarization direction was chosen to be in plane (p polarization) while no polarization analysis of the scattered light was made. The free spectral range chosen was 30 GHz and the usual backscattering geometry was used [10]. Even if no vertical slit was placed at the focusing–collecting lens, its dimensions were chosen to minimize the wavevector dispersion. In order to avoid photomultiplier damage, the elastic peak intensity was filtered using a JRS scanning-synchronized reference beam system.

X-ray absorption experiments were carried out at the EXAFS-3 beamline at the DCI storage ring of the Laboratoire pour l'Utilization du Rayonnement Electromagnetique (Orsay, France) with electron beam energy of 1.85 GeV and an average current of 250 mA. Data of the Ge K edge were obtained by using a fixed exit monochromator with two flat Si(311) crystals; detection was performed by collecting the total electron yield on a biased electrode in an He atmosphere sample chamber [11]. The experimental geometry was chosen in a manner that the x-ray polarization vector was normal to the surface of the sample and the incidence angle (formed between the incident x-ray wavevector and the surface) was about 5°. This grazing angle provides a detection of the XAS signal that comes about 1000 Å from the surface. It has been explained carefully elsewhere [12].

3. Results

3.1. Brillouin light scattering spectroscopy

Samples were placed on an automatic double goniometer which allowed the performance of two kinds of experiment: measurement of the azimuthal dispersion, involving variation of the angle α between the phonon propagation direction and the in-plane [110] direction of the SL (azimuthal angle), and measurement of the sagittal dispersion, involving variation of the angle θ between the incident (and scattered) beam and the normal to the surface. In sagittal dispersions the surface sound velocity obtained is plotted against the product kh (where k is the projection of the scattering vector on the sample's surface and h the total thickness of the layer). They yield the C_{44} elastic constant most sensitively through the Rayleigh mode, as well as the other elastic constants through the higher order Sezawa modes. These latter modes appear at critical values of kh for a 'soft' layer deposited on a 'hard' substrate [13].

Figure 1 shows typical spectra for these Si/Ge SL samples. The experimental peaks have been fitted with Gaussians in order to determine their positions respect to the elastic laser line. The Brillouin shifts are converted to sound velocities by $V^{SAW} = \nu_B/(2k_i \sin\theta_i)$ where V^{SAW} is the surface acoustic wave velocity, ν_B is the Brillouin shift and θ_i is the angle between the incident light and the normal to the surface. After that, a simulation program [14] was used to fit the dependence of the sound velocity in both sagittal and azimuthal experiments. This simulation program calculates the Brillouin spectrum of a layer of an opaque material over a substrate for light scattering by the ripple mechanism: details have been given elsewhere [14, 15]. In the first type of experiment, the adimensional quantity kh is changed by varying the angle of the incidence light on the sample and in the second one the measured surface phonon propagates along different crystalline directions when the sample turns around the (001) axis. Fits in both experiments were done by a trial-and-error method. Once a good fit had been obtained the effective elastic constants of the SL were varied arbitrarily up to a clear difference and the variation is taken as the error bar (which turned out to be practically the same for all of

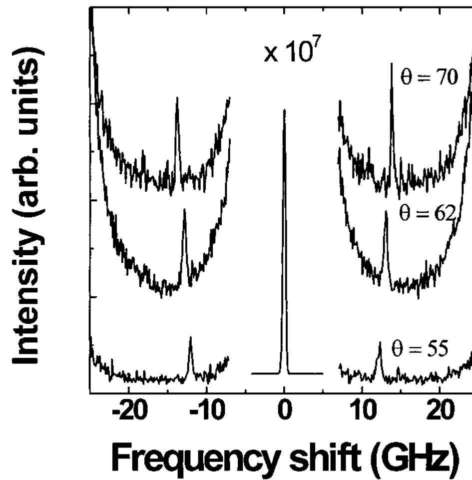

Figure 1. Brillouin light scattering spectra of $(Si_5/Ge_5)_{217}$ SL with the phonon propagating along the [100] direction at several sagittal angles.

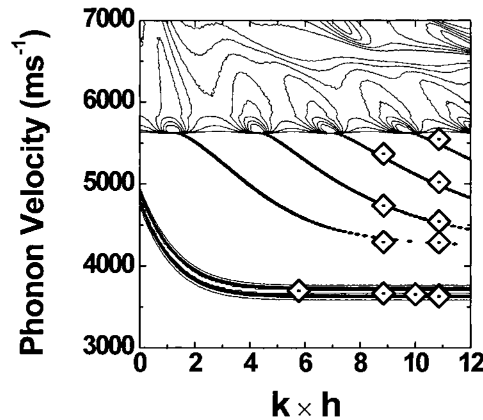

Figure 2. Brillouin intensity as a function of the surface wave phase velocity and kh for an $(Si_{20}/Ge_{20})_{55}$ SL with the phonon propagating along the [100] direction. Diamonds represent experimental points and lines and contours are calculations based on effective elastic constants of the superlattice.

them and always less than 1 GPa). The spectrum can be simulated either for different values of kh, which gives the sagittal dispersion, or for different phonon propagation directions in the surface, giving the azimuthal dispersion. The calculations correspond to three-dimensional graphs whose usual representation is a contour plot. In these plots the most intense zones correspond to the peaks and are plotted as white or black lines, which correspond to either Rayleigh or Sezawa modes. In figure 2, a sagittal fit for the $(Si_{20}/Ge_{20})_{55}$ superlattice with the phonon propagating along the [100] direction is presented. Squares are the experimental points and lines and contours are calculations based on effective elastic constants of the superlattice. Note the cutoff near $V \approx 5600$ m s^{-1} at the transonic state or transverse velocity threshold of the Si(001) substrate. As well as the pseudo-surface-wave precursors above this threshold, which are Sezawa-like modes, leak energy into the substrate is seen as intense spots whose intensity decays as the velocity increases forming a flamelike contour.

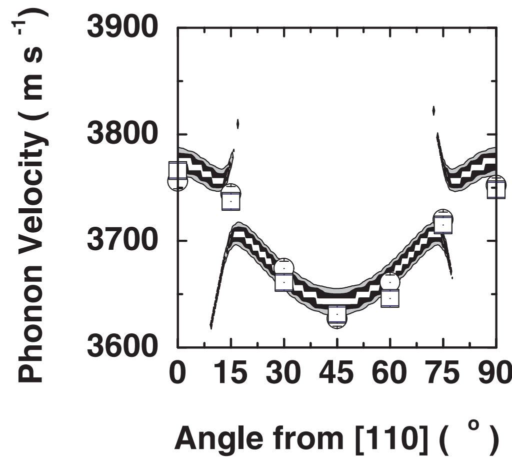

Figure 3. Azimuthal dispersion of an $(Si_{32}/Ge_8)_{60}$ superlattice at $kh = 10.86$. Circles and squares represent fits to the Rayleigh-like peaks of the experimental spectra taken in different experiments (so as to assess the reproducibility of the results). Lines are a contour plot of the azimuthal dispersion calculation based on effective elastic constants of the superlattice.

Bearing in mind the common observation that elastic constants obtained by BLS are slightly lower than those measured by ultrasounds [16, 17], we have measured the C_{ij} of Si and Ge single crystals by BLS in order to compare measurements and predictions for the effective elastic constant tensor of Si/Ge superlattices.

Next we determined the elastic constant tensor of the Si/Ge SLs, by measuring sagittal dispersions with the phonon propagating along the crystallographic [100] and [110] directions, as well as azimuthal dispersions, in order to be sure of our results. Measurements were repeated in geometries to assess the reproducibility of our experimental results. In figure 3, the azimuthal dispersion of the $(Si_{32}/Ge_8)_{60}$ superlattice at $kh = 10.86$ is presented. Circles and squares are fits to the Rayleigh-like peaks of the spectra taken in different experiments. The line is the contour plot of the corresponding azimuthal dispersion calculation. The elastic constant values for the SLs are listed in table 1. Only the C_{44} values are reported for $(Si_{12}/Ge_4)_{80}$ and $(Si_4/Ge_{16})_{120}$ samples because this is the more easily obtained by BLS and because main conclusions can be obtained by taking into account only this elastic constant.

We need also to point out that, in interpreting the measured data, we have assumed that the elastic constant tensor of the SL has cubic symmetry with three independent constants. The long wavelength limit is assumed, and an effective elastic constant tensor (C_{ij}^{Eff}) thereby derived. This tensor is related to the C_{ij} of bulk Si and Ge and the atomic fractions f_{Si} and f_{Ge}:

$$\frac{1}{C_{ij}^{Eff}} = \frac{f_{Si}}{C_{ij}^{Si}} + \frac{f_{Ge}}{C_{ij}^{Ge}}. \tag{1}$$

When this tensor is calculated by the Grimsditch–Nizzoli approach for our SLs [18], it has the form appropriate to a tetragonal medium, displaying six independent elastic constants. However, with regard to the numerical values obtained, the differences between C_{12} and C_{13}, C_{11} and C_{33}, C_{44} and C_{66} are so slight that simplifying this tensor to a cubic form does not imply a loss of accuracy. For the $(Si_{20}/Ge_{20})_{55}$ SL (and almost equivalently for the rest of the samples), for example, before being equated, the distinct elastic constants are: $C_{11} = 141.7$ GPa versus $C_{33} = 139.6$ GPa, $C_{12} = 53.2$ GPa versus $C_{13} = 52.6$ and

Table 1. Values of the elastic constants (C_{ij}^{Eff}) for Si_m/Ge_n superlattices: Experimentally obtained in the present work by BLS (C_{ij}^{Eff}(Exp)). Values calculated by the Grimsditch–Nizzoli approach (C_{ij}^{Eff}(GN)); propagated error for these values is approximately 1 GPa. Deviation between the experimental C_{ij}^{Eff} values and those calculated by the Grimsditch–Nizzoli approach ($\Delta(C_{ij}^{Eff})$) (the percentage has been calculated as $\Delta(C_{ij}^{Eff}) = 100(C_{ij}^{Eff}(\text{Exp}) - C_{ij}^{Eff}(\text{GN}))/C_{ij}^{Eff}(\text{GN})$).

	C_{ij}^{Eff}(Exp)			C_{ij}^{Eff}(GN)			$\Delta(C_{ij}^{Eff})$		
Sample	C_{11} (GPa)	C_{12} (GPa)	C_{44} (GPa)	C_{11} (GPa)	C_{12} (GPa)	C_{44} (GPa)	ΔC_{11} (%)	ΔC_{12} (%)	ΔC_{44} (%)
$(Si_4/Ge_{16})_{120}$			64 ± 1			69.0			−7
$(Si_{20}/Ge_{20})_{55}$	159 ± 1	56 ± 1	69 ± 1	141.7	53.2	69.5	12	5	0
$(Si_{15}/Ge_{15})_{73}$	161 ± 2	56 ± 1	70 ± 1	142.0	53.4	69.7	13	5	0
$(Si_{10}/Ge_{10})_{110}$	162 ± 2	56 ± 1	70 ± 1	141.7	53.2	69.5	14	5	0
$(Si_5/Ge_5)_{217}$	158 ± 1	56 ± 1	70 ± 1	141.3	53.0	69.4	12	5	0
$(Si_{12}/Ge_4)_{80}$			75 ± 1			76.0			0
$(Si_{32}/Ge_8)_{60}$	154 ± 1	58 ± 1	72 ± 1	156.4	59.5	74.3	−1	−2	−3
$(Si_{16}/Ge_4)_{120}$	157 ± 1	60 ± 1	74 ± 1	157.2	59.8	74.6	0	0	0

$C_{44} = 69.5$ GPa versus $C_{66} = 70.0$ GPa. Bearing in mind that the uncertainty in the elastic constant determination $\Delta C_{ij} = 1$ GPa, our approach of restricting the elastic constant tensor to its cubic crystal form is reasonable.

We note also that previous work on Si/Ge SLs was restricted to C_{44}. They reported good agreement between calculated and experimental values of this constant [19, 20]. The present results are fully compatible with those previous ones, since it is only for C_{33} that an unexpected value is found, while for C_{44} the predictions are in good agreement with experiment.

3.2. X-ray absorption spectroscopy

We have performed EXAFS experiments at the Ge K edge on these superlattices. Following the standard procedure [21], the $\chi(k)$ EXAFS signal has been obtained after the subtraction of the atomic background, which is fitted by a cubic spline polynomial. Figure 4 shows the EXAFS signal of several superlattices obtained after normalization by the jump edge. Also shown for comparison are the spectrum of pure Ge and of an Si-rich $Si_{1-x}Ge_x$ thin film alloy. Obviously, the first one has only Ge–Ge and the latter $Si_{1-x}Ge_x$ alloy has mainly Ge–Si contribution to the EXAFS spectra. At first sight, taking into account the shape of the backscattering amplitude for Ge and Si [21], the Ge one has a deep minimum at 4 Å^{-1} which is just the maximum in the Si amplitude. Thus, the height of the oscillation at 4 Å^{-1} may be considered as a semi-quantitative indicator for the relative amount of Si in the first coordination shell as has been done for the study of Si/Ge alloys [22]. Based on the deep minimum for Ge and the maximum for Si backscattering amplitudes, it can be observed in figure 4 for these samples that the EXAFS signal is sensitive to the number of Ge–Si bonds and that the number of Si atoms present at the first coordination shell is not negligible at all, even for samples with thick Ge layers.

Let us define an 'ideal superlattice' as one which has abrupt interfaces between layers and, consequently, does not present interdiffusion between layers of different elements. For that ideal superlattice each atom of germanium being at the interface would have two Ge neighbours inside the Ge layer and two Si neighbours from the adjacent Si layer. From this model one can say that in ideal superlattices with the composition of our samples, the main coordination number (CN) of Ge ranges from 3.0 atoms of Ge and 1.0 of Si (for the Si_{16}/Ge_4 superlattice) to

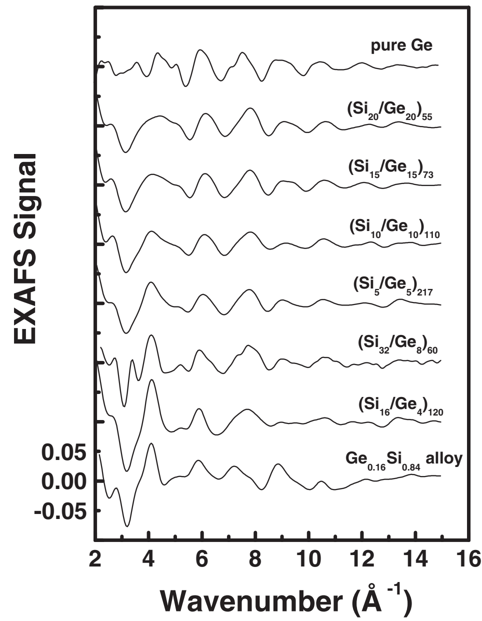

Figure 4. Experimental Ge K-edge EXAFS signal of several samples after atomic background subtraction.

3.8 atoms of Ge and 0.2 of Si (for the Si_{20}/Ge_{20} superlattice). CNs for these ideal superlattices are reported in table 2. From these CNs, it seems that the Ge–Si contribution to the EXAFS signal must be very small and similar in all studied samples. Nevertheless, by looking the obtained EXAFS signal, this seems not to be the case in the measured spectra, where appreciable oscillations are present at 4 $Å^{-1}$ and where there are big differences between samples.

In order to obtain the Ge–Ge and Ge–Si distances and coordination numbers, a quantitative analysis of the EXAFS data has been carried out. We used a PC-computer program developed by Bonnin *et al* [23]. The filtered EXAFS oscillations, $\chi(k)$, are fitted to the well known expression [21]

$$\chi(k) = S_0^2 \sum_j \frac{3N_j \cos\Theta_j}{kR_j^2} \, e^{-2k^2\sigma_j^2} \, e^{\frac{-\Gamma_j R_j}{k}} \, f_j(k) \sin[2kR_j + \phi_j(k)] \tag{2}$$

which describes the EXAFS oscillations for a distribution of atoms around the absorber, considering single scattering and the plane-wave approximation. S_0^2 is an inelastic loss reduction factor, N_j is the average coordination number for the Gaussian distribution of distances centred at the R_j value, Θ_j is the angle between the x-ray polarization and the bond direction. In our samples there is no polarization effect because of the particular Ge structure. That crystallographic structure means that single crystalline samples have the same EXAFS signal as the polycrystalline ones because $\sum_j(3N_j \cos\Theta_j) = 1$. σ_j is the Debye–Waller factor, and $\phi_j(k) = 2\delta(k) + \gamma_j(k)$ is the phase shift, $\delta(k)$ and $\gamma_j(k)$ being the central and backscattering atom phase shifts, respectively. $f_j(k)$ is the magnitude of the backscattering amplitude of the jth neighbour atom and k/Γ_j is a convolution of the mean free path of the photoelectron travelling from the absorbing atom to the backscatterer in the jth shell and the lifetime of the core hole.

Table 2. Summary of coordination numbers, distances and Debye–Waller factors obtained from fits by equation (2) for Ge, K-edge EXAFS spectra; the S_0 inelastic loss factor has been obtained by fitting two references. The coordination number for an ideal superlattice with abrupt interfaces is given for comparison. (Numbers in parentheses are the experimental incertitude in the last digit.)

Sample	Pair	N_{ideal}	N/S_0^2 (fit)	R_j (Å)	σ^2 ($\times 10^{-3}$) (Å^2)
Ge	Ge–Ge	4.0	$S_0^2 = 0.7$	2.44	2.5
$Ge_{0.16}Si_{0.84}$	Ge–Ge	0.64	$S_0^2 = 0.7$	2.44(1)	3.6
	Ge–Si	3.36	$S_0^2 = 0.8$	2.34(1)	
Si_4/Ge_{16}	Ge–Ge	3.75	0.7(1)	2.46(1)	2.5
	Ge–Si	0.25	2.9(4)	2.32(1)	
Si_{20}/Ge_{20}	Ge–Ge	3.8	2.7(2)	2.45(1)	2.5
	Ge–Si	0.2	1.3(4)	2.32(1)	
Si_{15}/Ge_{15}	Ge–Ge	3.73	2.5(2)	2.44(1)	2.5
	Ge–Si	0.27	1.2(4)	2.35(1)	
Si_{10}/Ge_{10}	Ge–Ge	3.6	1.7(1)	2.45(1)	2.5
	Ge–Si	0.4	1.3(4)	2.34(1)	
Si_5/Ge_5	Ge–Ge	3.2	1.9(1)	2.46(1)	2.5
	Ge–Si	0.8	1.0(4)	2.34(1)	
Si_{12}/Ge_4	Ge–Ge	3.0	2.8(2)	2.41(1)	2.5
	Ge–Si	1.0	0.9(3)	2.41(1)	
Si_{32}/Ge_8	Ge–Ge	3.5	1.9(2)	2.42(1)	2.5
	Ge–Si	0.5	2.0(3)	2.42(1)	
Si_{16}/Ge_4	Ge–Ge	3.0	1.2(1)	2.44(1)	2.5
	Ge–Si	1.0	1.5(3)	2.44(1)	

Figure 5 shows the Fourier transform of the $k^3\chi(k)$ weighted EXAFS signal: this is a picture of the radial distribution function around the Ge atoms. In the following, we will concentrate on the information contained in the peak appearing around 2 Å, which is related to the first coordination sphere, including the Ge–Ge and Ge–Si contributions.

In order to perform the fits, the backscattering functions have been calculated by using the FEFF code version 6.01 reported by Rehr [24]. For that calculation, two different clusters have been considered to obtain the Ge–Ge and Ge–Si contributions. Clusters were built by a central Ge atom surrounded by four Ge (or Si) neighbours in a tetrahedral symmetry as in a pure Ge environment structure (or pure Si). In order to test the Ge–Ge and Ge–Si amplitude and phase backscattering functions and also to evaluate the S_0 reduction factor, a pure Ge sample and a Si–Ge thin film alloy (with 16% of Ge) have been taken as references.

A two-shell fit has been performed in order to reproduce the experimental signal. Following a similar procedure to the simultaneous analysis proposed by Aebi *et al* [25], some conditions have been imposed on the fit: the S_0^2 factor has been fixed to be equal to the value corresponding to a pure Ge crystal. At no time was the number of fitting parameters greater than the maximum number allowed by the Nyquist theorem (i.e. $N_{idp} = (2\Delta k\Delta R)/\pi$) which is accepted by the EXAFS Standard and Criteria [26]. In our case $\Delta R = (2.8\text{–}1.6)$ Å, $\Delta k = (14.95\text{–}3.5)$ Å^{-1} and $N_{idp} = 8.8$. The quality of the fits was judged by a least squares fitting parameter. In order to illustrate the quality of the fit, figure 6 shows the k^3-space and the distance-space comparisons between the filtered EXAFS signal and the calculated one for one particular sample. Table 2 summarizes the parameters of equation (2) that better fit the experimental data.

It can be observed that the contribution of Ge–Si pairs is much more important than expected from the above-described ideal model. From these results, one can conclude that the

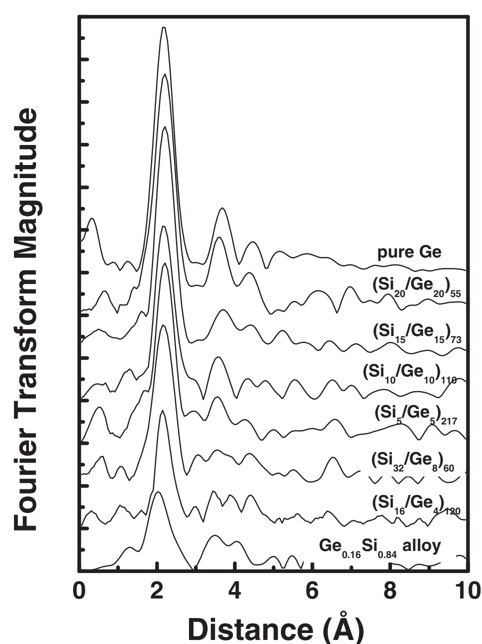

Figure 5. Fourier transform magnitude of several Si/Ge superlattices.

Si–Ge interfaces are not so perfect as could be expected and that the interdiffusion is much higher than that corresponding to abrupt interfaces. These results are in agreement with the long range order characterization carried out by x-ray diffraction [27] and give the key to understand the way the Si–Ge interaction may become important to understand the elastic properties.

On the other hand, from the distance point of view, samples can be classified into two types. In the first one (Si_n/Ge_n and Si_n/Ge_{4n} samples), the obtained distances show a non-relaxing Ge–Ge distance very similar to that corresponding to pure Ge (2.45 Å); the Ge–Si distance is much shorter (around 2.34 Å) and similar to the Si–Si distance in pure Si. This effect is similar to that observed in Si_xGe_{1-x} alloys [28], where the Ge–Ge distance is 2.445 Å and the Ge–Si one is 2.40 Å independent of the alloy composition. In contrast, fits for $(Si_{16}/Ge_4)_{120}$, $(Si_{32}/Ge_8)_{60}$ and $(Si_{12}/Ge_4)_{80}$ samples give Ge–Si distances equal to the Ge–Ge ones, which can be relaxed depending on the sample. Due to the particular symmetry of the Ge structure, even polarization dependent EXAFS spectroscopy [12] cannot give information about whether compression is present mainly in the in-plane or in the out-of-plane direction.

These results seems to be in disagreement with the distances obtained in Ge_n/Si monolayers where no Ge bulklike distances have been found for $n < 8$ (n is the number of atomic monolayers [29]). Superlattices would be different structurally from the ultrathin single layers, in that there is more interdiffusion between Ge and Si layers and that there are no relaxations from the bulk distances. From our point of view, these results should be taken into account in order to interpret the optical characterization of the samples, where for example, it has been reported that superlattices with different modulation wavelengths exhibit different photoluminescence spectra [30].

Summarizing, it seems clear that Si_n/Ge_m (with $n \leqslant m$) samples: firstly, from their x-ray diffraction data [20] and their cross sectional transmission electron microscopy [31], present a

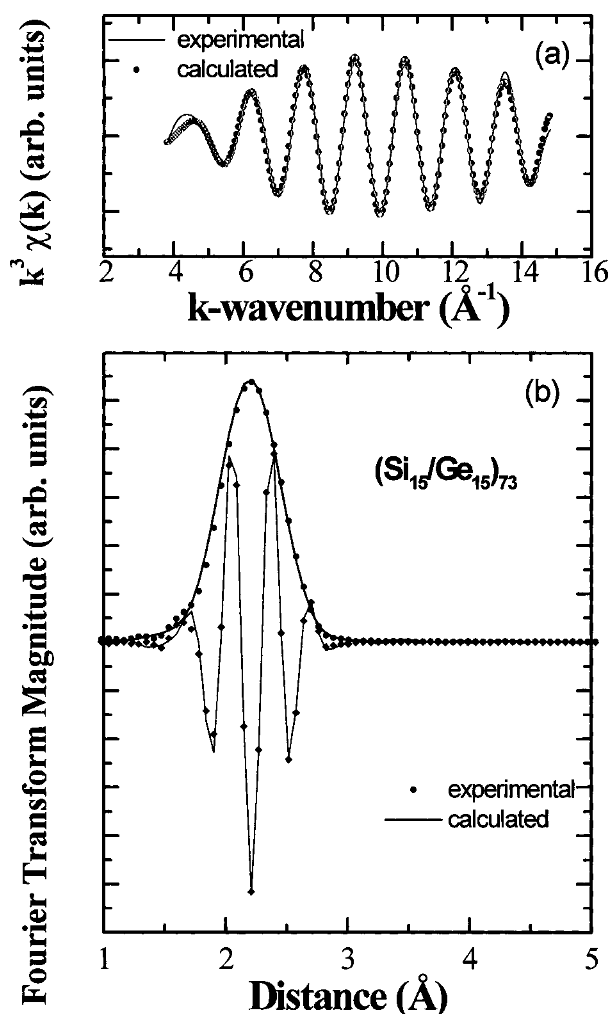

Figure 6. (a) k^3-space comparison between the experimentally obtained $\chi(k)$ EXAFS signal and the calculated function by equation (2) with the parameters given in table 1. (b) Fourier transform modulus and imaginary part comparisons of the same EXAFS signal.

much higher degree of interdiffusion at the interface; and secondly and more important, from EXAFS data, the material forming the interface can be considered as an alloy that is structurally compressed. But, Si_n/Ge_m (with $n > m$) samples have a small degree of interdiffusion (that means sharp interfaces) and the material forming the interface is relaxed and structurally behaves as a bulk Si_xGe_{1-x} alloy.

A schematic picture to illustrate the EXAFS results is presented in figure 7. (a) shows an ideal superlattice (sharp interfaces), having elements with different lattice parameters from the Si/Ge ones. In (b), that superlattice becomes a sample with less abrupt interfaces. At the interface has been plotted an SiGe alloy with a Ge–Si distance equal to the Si–Si one in pure Si. That interface model can be considered as a Si lattice that includes Ge atoms, where the bigger size of Ge does not provide an increase of the lattice parameter, as in a bulk Si–Ge alloy. Probably the long range order of this alloy becomes slightly distorted (this has been

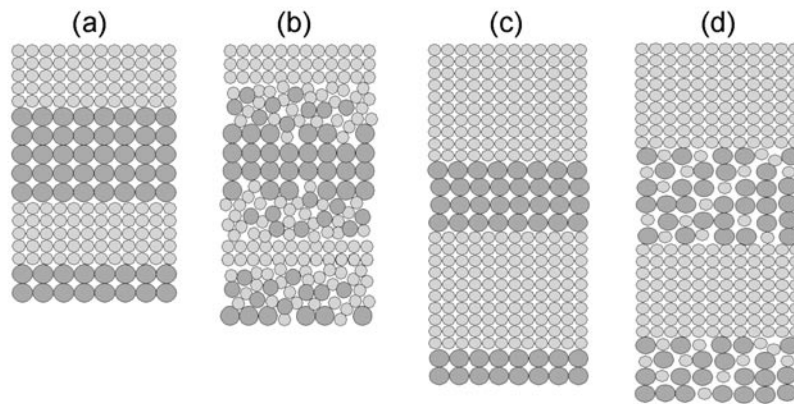

Figure 7. Schematic plot of two types of interface in Si/Ge superlattices (see text).

represented also in the figure). In this sample, the Ge–Ge distance in the Ge layer remains equal to the bulk germanium. On the other hand, (c) and (d) show the modelization of a superlattice sample with Ge layers thinner than Si ones. In (d) the alloy forming the interface (and also the Ge layer) can be considered a Ge lattice having Si atoms inside. The Ge–Si distance is equal to the Ge–Ge one and they are dependent of the relative concentration; this alloy relaxes to smaller distances depending on the degree interdiffusion.

4. Discussion

The aim of our study has been to relate the match or mismatch between the experimental results of the predictions of continuum elasticity theory to the microstructure of our samples. The long wavelength limit is assumed, and an effective elastic constant tensor (C_{ij}^{Eff}) is obtained by using equation (1), where atomic fractions have been obtained the by x-ray reflectivity [20].

The three last columns in table 1 give the difference between the experimental values (Exp) and those calculated by the Grimsditch–Nizzoli approach (GN), normalized to the latter. It must be said that since the C_{ij}^{Eff} are calculated from the experimental values of the C_{ij} for Si and Ge (in which the maximum uncertainty was $\Delta C_{ij} = 1$ GPa), the error in the predictions will be approximately 1 GPa as well.

The results presented in table 1 can be divided into two groups. One group corresponds to the Si_{4n}/Ge_n and to the Si_{3n}/Ge_n SLs. In these samples the predictions of elasticity theory are in very good agreement with experiment, providing experimental support for the Grimsditch–Nizzoli approach for calculating the C_{ij}^{Eff} of structurally perfect systems. These samples are found to be almost long range structurally perfect: they have very sharp interfaces, no strain (a perfect lattice match with the buffer) and a low number of defects. Moreover, in the case of the $(Si_{32}/Ge_8)_{60}$ sample, that has interfaces as sharp as the $(Si_{16}/Ge_4)_{120}$ one, but a higher number of defects, the predictions are slightly lower than experiment, which could result from the presence of these defects.

On the other hand, for the Si_n/Ge_n and Si_n/Ge_{4n} SLs, the measured values of C_{33} (or C_{11} in the cubic approach) exceed the calculated ones by up to 14%. A slight excess in the measured value of C_{12} of around 5% can be observed.

This classification is in coincidence with that made after the analysis of the EXAFS data, which provides two different kinds of sample: one of them with the same Ge–Ge and Ge–Si distances and the other with different values for those distances. That classification allows two

types of Si_n/Ge_m sample with different interfaces. Interfaces in samples with $n \leqslant m$ can be explained as formed by a compressed Si–Ge alloy because the Ge–Si distances are equal to the atomic Si–Si ones. Interfaces in samples with $n > m$ are formed by a relaxed Si–Ge alloy because the Ge–Si distances are equal to that obtained for the Ge layer at the superlattice.

Sklar *et al* [32] have shown that the most important elastic constant change of a stressed layer is due to the strain. They have calculated a decrease of 4%, 0% and 12% from the bulk values of C_{11}, C_{12} and C_{44} elastic constants, respectively, for a GaAs layer subjected to a perpendicular strain of 0.4%. Those data are not so different from our results because the mismatch for Si/Ge superlattices is similar to that strain and the observed relative variations of the elastic constants are of the same order. Bearing in mind this effect, it is very easy to justify the discrepancy between the experimental elastic constant values and those calculated by the theory of the elasticity. Samples having interfaces formed by compressed SiGe alloy present anomalous elastic values. The discrepancy percentage is of the order of that reported for a strained GaAs layer.

5. Conclusions

The full set of elastic constants of Si_m/Ge_n superlattices has been determined by Brillouin light scattering spectroscopy. Moreover, their elastic constants have been calculated by the continuum elasticity theory based on the experimental values of the bulk Si and Ge elastic constant, which has been measured under the same experimental conditions.

The experimental values of the C_{11} elastic constant of Si_n/Ge_n and Si_n/Ge_{4n} superlattices (n is the number of monolayers) are higher than expected from the continuum elasticity theory. On the other hand, Si_{4n}/Ge_n and Si_{3n}/Ge_n superlattices match perfectly the theoretical predictions. The observed difference between them has been explained from a microstructural point of view based on the EXAFS characterization. Si_{4n}/Ge_n and Si_{3n}/Ge_n superlattices have interfaces formed by a relaxed SiGe alloy that do not alter the elastic constant values of the superlattice. Nevertheless, Si_n/Ge_n and Si_n/Ge_{4n} superlattices have interfaces formed by a compressed SiGe alloy that do alter the elastic constant values.

Acknowledgments

We are grateful to Professor V R Velasco for helpful discussions. Thanks are given to the staff in charge of LURE for technical assistance during x-ray absorption experiments. This work has been supported by the CICyT under contract number MAT97-0725.

References

[1] Fasol G, Fasolino A and Lugli P (ed) 1989 *Spectroscopy of Semiconductor Microstructure* (New York: Plenum)
[2] Okamura H, Miki K, Sakamoto K Sakamoto T, Endo K and Yoshida S 1989 *Appl. Surf. Sci.* **41/42** 548
[3] Schuller I K, Fartash A and Grimsditch M 1990 *MRS Bull.* **15** 33
[4] Tsakalakos T and Hilliard J E 1982 *J. Appl. Phys.* **48** 876
[5] Sakaue F *et al* 1993 *J. Magn. Magn. Mater.* **126** 207
[6] Grimsditch M and Schuller I K 1991 *Surface Science* ed F A Ponce and M Cardona (Berlin: Springer)
[7] de Bernabé A, Prieto C, González L, González Y and Every A 1999 *J. Phys.: Condens. Matter* **11** L331
[8] Arbet V, Chang S J and Wang K L 1989 *Thin Solid Films* **183** 57
[9] Sandercock J R 1982 *Light Scattering in Solids III* ed M Cardona and G Guntherdot (Berlin: Springer)
[10] Mutti P, Bottani C E, Ghislottie G, Beghi M, Briggs G A D and Sandercock J R 1995 *Advances in Acoustic Microscopy* vol 1 ed G A D Briggs (New York: Plenum)
[11] Tourillon G, Dartyge E, Fontaine A, Lemonnier M and Bartol F 1987 *Phys. Lett.* A **121** 251

[12] Castañer R, Prieto C, de Andrés A, Martínez J L, Martínez-Albertos J L, Ocal C and Miranda R 1994 *J. Phys.: Condens. Matter* **6** 4981
[13] Farnell G W and Adler E L 1972 *Physical Acoustics* vol 9 ed W P Mason and R W Thurston (New York: Academic) ch 2
[14] Zang X, Comins J D, Every A G, Stoddart P R, Pang W and Derry T E 1998 *Phys. Rev.* B **58** 13 677
Sandercock J R 1978 *Solid State Commun.* **26** 547
[15] Marvin A, Bortolani V, Nizzoli F and Santoro G 1980 *J. Phys. C: Solid State Phys.* **13** 1607
[16] Sandercock J R 1978 *Solid State Commun.* **26** 547
[17] Velasco V R and García-Moliner F 1980 *Solid State Commun.* **33** 1
[18] Grimsditch M and Nizzoli F 1986 *Phys. Rev.* B **33** 5891
[19] Mendik M, Ospelt M, von Känel H and Wachter P 1991 *Appl. Surf. Sci.* **50** 303
[20] de Bernabé A and Prieto C 1997 *Surf. Interface Anal.* **25** 324
de Bernabé A, Jiménez R, García-Hernández M and Prieto C 1998 *Thin Solid Films* **317** 255
[21] See for instance: Teo B K 1986 *EXAFS. Basic Principles and Data Analysis* (Berlin: Springer)
Koningsberger D C and Prins R 1988 *X-ray Absorption Principles, Applications, Techniques of EXAFS, SEXAFS and XANES* (New York: Wiley)
[22] Aebi P, Tyliszczak T, Hitchcock A P, Jackman T E and Baribeau J M 1991 *J. Vac. Sci. Technol.* A **9** 907
[23] Bonnin D, Kaiser P and Desbarres J EXAFS PC-software *8th Europhys. School on Chemical Physics (La Rabida, 1992)*
[24] Rehr J J 1993 *Japan. J. Appl. Phys.* **32** 8
[25] Aebi P, Tyliszczak T, Hitchcock A P, Baines K M, Sham T K, Jackman T E, Baribeau J M and Lockwood D J 1992 *Phys. Rev.* B **45** 13 579
[26] Report on the International Workshop on Standard and Criteria in XAFS *X-ray Absorption Fine Structure* ed S S Hasnain (Chichester: Ellis Horwood 1991) p 751
[27] de Bernabé A, Prieto C, Cáceres D, Vergara I, Every A G and Fischer H E *Phys. Rev.* B at press
[28] Kajiyama H, Muramatsu S, Shimada T and Nishino Y 1992 *Phys. Rev.* B **45** 14 005
[29] Oyanagi H, Sakamoto T, Sakamoto K, Yamaguchi H, Yao T, Kuwahara Y and Matsushita T *X-ray Absorption Fine Structure* ed S S Hasnain (Chichester: Ellis Horwood, 1991) p 238
[30] Okumura H, Miki K, Sakamoto K, Endo K and Yoshida S 1989 *Appl. Surf. Sci.* **41/42** 548
[31] Adams P M, Bowman R C, Ahn C C, Chang S J, Arbet-Engels V, Kallel M A and Wang K L 1992 *J. Appl. Phys.* **71** 4305
[32] Sklar Z, Mutti P and Briggs G A D 1995 *Review of Progress in Quantitative Nondestructive Evaluation* vol 14 ed D O Thompson and D E Chimenti (New York: Plenum)